Nonlinear Dyn (2021) 105:371–386
https://doi.org/10.1007/s11071-021-06606-w

ORIGINAL PAPER

Observer-based continuous adaptive sliding mode control for soft actuators

Guizhou Cao · Yanhong Liu · Yichen Jiang · Fangfang Zhang · Guibin Bian · David H. Owens

Received: 18 December 2020 / Accepted: 4 June 2021 / Published online: 16 June 2021

Abstract Fabricated by high elastic materials, soft actuators provide a prominent solution for soft rehabilitation gloves, soft graspers and locomotion robots. However, the control of soft actuators is a grant challenge due to dynamic modeling error and unavailable system states. This paper proposes an observer-based continuous adaptive sliding mode controller for soft actuators in the presence of system uncertainties without knowledge of its upper bound in prior. By exploiting a novel nonsingular fast terminal sliding mode (NFTSM) surface and a high-order sliding mode (HOSM) observer, the proposed control scheme features adaptive-tuning gains, continuity, singularity-free, stronger robustness and higher tracking accuracy. The stability of the proposed controller is analyzed by the Lyapunov method. Corresponding comparative simulations and experiments of a soft pneumatic network actuator verify the effectiveness and related features of the proposed controller.

Keywords Adaptive robust control · Soft actuator · Nonsingular fast terminal sliding mode surface · Super-twisting algorithm · High-order sliding mode observer · Pneumatic network actuator

G. Cao · Y. Liu (✉)· Y. Jiang · F. Zhang · G. Bian · D. H Owens
School of Electrical Engineering, Zhengzhou University, Zhengzhou 450001, People's Republic of China
e-mail: liuyh@zzu.edu.cn

G. Cao
State Grid Henan Electric Power Research Institute, Zhengzhou 450000, People's Republic of China

G. Bian
Institute of Automation, Chinese Academy of Sciences, Beijing 100190, People's Republic of China

David H Owens
Department of Automatic Control and Systems Engineering, University of Sheffield, Sheffield, UK

1 Introduction

Soft actuators bring a state-of-the-art solution for vigorous applications, such as soft gloves [1,2], knee assistive devices [3] and soft bio-inspired fishes [4] due to the inherent flexibility, safety and adaptivity [5]. In most applications, velocity is generally required by feedback control laws for high-precision position control. In the case of rigid robots, the velocity information can be accurately measured by solid-state sensors, such as tachometers, speedometers and gyroscopes. However, these rigid velocity sensors cannot be installed on soft actuators due to the damage to their characters, such as flexibility, safety [6]. Moreover, the flexibility, stepping from the high-dimensional continuous deformation of soft materials, impedes an accurate dynamic model of soft actuators. The system uncertainties, including unmodeled dynamics, external disturbance, should be practically considered in controller design. Therefore, both lacking state information and containing unavoidable uncertainties congregate on the position control obstacles of soft actuators.

The observer-based robust control method is one of the most applicable control schemes for soft actuators. Although some famous controllers and observers, including neural network controller [7], online learning controller [8], the Luenberger observer [9], have been successfully utilized on the soft actuators, sliding mode controllers (SMCs) have captured particular attention due to well-known robustness [10–12]. For example, Khawwaf et al. adopted an extended state observer to estimate lumped system uncertainties, and then, a linear SMC and a nonsingular terminal SMC were separately addressed to assure the system robustness [13]. Wang et al. employed the radial basis function neural network to estimate the unmodeled dynamics and system states and proposed a linear SMC for the trajectory tracking control for dielectric elastomer actuators [14]. For better control performances, existing observer-based SMCs remain vulnerable to be improved by three aspects: continuity, adaptivity and finite-time stability.

The discontinuous controller induces the chattering phenomenon, and this phenomenon not only increases the risk of equipment failure but also motivates the unmodeled dynamics at high frequency. To eliminate the chattering phenomenon, the super-twisting algorithm (STA) enables second-order sliding mode controllers one of the most applicable controllers due to continuous control signal, finite-time convergence of sliding variance and Lipschitz uncertainty/perturbation compensation [15]. Due to these features, the STA is widely used as controllers and observers, and it has been successfully utilized as a direct torque controller for a variable-flux memory machine [16] and a boost inverter observer for a hybrid PV-battery system [17]. However, the continuity of the second-order sliding mode control scheme will not be achieved if one simultaneously adopts an STA-based observer (STO) and an STA-based controller (STC) [15,18].

The adaptivity of robust controllers releases the prior knowledge of upper bounds of system uncertainties, which is difficult to be priorly known in practice [19,20]. The adaptivity of STC has been also investigated to tackle this engineering problem lying in lots of applications, such as automatic carrier landing of aircraft [21], space debris capturing [22], projective synchronization of flexible manipulator [23] and robot manipulators [24]. Despite this, it is of great importance to employ the adaptive observer-based STC to soft actuators for improving system performances.

Compared with asymptotically stable systems, the finite-time stabilizing closed-loop systems usually show stronger robustness properties [25]. To improve convergence rate on the sliding mode surface, a terminal sliding mode surface [26] and a fast terminal sliding mode (FTSM) surface [27] were, respectively, employed for microgrid and spacecraft simulations. Although the convergence rate of system states on the (fast) terminal sliding mode surface is faster than the linear sliding mode surface, the singularity may be the biggest obstacle for physical applications [28]. To tackle the singularity problem and meanwhile guarantee the finite-time convergence of system states on the sliding surface, a nonsingular terminal sliding mode surface and a nonsingular FTSM (NFTSM) surface have been investigated and utilized for various applications recently, such as noncooperative target spacecrafts [29], unmanned aircraft systems [30] and redundantly parallel mechanism systems [31]. It should be noted that the robustness of the sliding mode controller mainly lies in the sliding phase, where the sliding mode surface is insensitive to system perturbations and disturbance [32,33]. But on the reaching phase, the robustness of SMC is the same as other controllers. Along this line of thought, the convergence rate of the sliding variance under the NFTSM is slowed down by a feedback term, which induces that the robustness of the closed loop is degraded [34,35]. Furthermore, the STA is difficult to be applied on the NFTSM surface.

To the authors' best knowledge, the integration of continuity, adaptivity and finite-time stability of observer-based SMC schemes is still open. This paper is focused on observer-based continuous adaptive sliding mode control for soft actuators, and the main contributions are summarized as follows.

- A novel tracking control scheme is proposed for soft bending actuators, and it features continuity, adaptivity, singularity-free, without velocity measurements and stronger robustness.
- By exploiting a novel sliding mode surface s, an improved STC is designed with adaptive-tuning gains and a faster convergence rate of s, while the upper bound of system uncertainties is not required in prior.
- Tracking errors of the closed-loop system converge to zero, rather than predefined manifold, and it is proved by the Lyapunov method.

- Corresponding comparative simulations and experiments on a pneumatic network actuator verify the effectiveness of the proposed control scheme.

The rest of the paper is organized as follows. Section 2 presents the dynamic model of soft actuators in the form of the Euler–Lagrangian equation and describes the control problem. In Sect. 3, the proposed control scheme is constructed, and the stability is proved under the Lyapunov method. In Sect. 4, the proposed control scheme is analyzed to show the corresponding features. In Sect. 5, comparative simulations and experiments show the effectiveness of the proposed controller. Finally, Sect. 6 concludes this paper.

2 Model description and problem statement

Based on the Euler–Lagrangian method, the dynamic model of soft bending actuators can be described as [36,37],

$$M(q)\ddot{q} + C(q,\dot{q})\dot{q} + G(q) = u + d_0, \tag{1}$$

where $q, \dot{q} \in \mathcal{R}^{n\times 1}$ are the bending angle and velocity of the actuator, respectively. $M(q)$, $C(q,\dot{q})$, $G(q)$ are the inertia matrix, the centripetal and Coriolis matrix and the gravitational force and stress matrix, respectively. u is the control input, and d_0 denotes lumped system uncertainties including external disturbance, unmodeled dynamics and parameter variations.

As one of the mechanical systems, soft actuators also satisfy the following mechanical properties for each $q, \dot{q}$ [36,37].

Property 1 The inertia matrix $M(q)$ is symmetrical and positive definite.

Property 2 $\dot{M}(q) - 2C(q,\dot{q})$ is a skew-symmetric matrix, such that $x^T\left(\dot{M}(q) - 2C(q,\dot{q})\right)x = 0$ for each $x \in \mathbb{R}^{n\times 1}$.

Property 3 Since $C(q,\dot{q})$ is bounded in q and linear in $\dot{q}$, then one has

$$\begin{aligned} &||C(q,\dot{q})|| \le K_c||q||, \\ &C(q,\dot{q})x = C(q,x)\dot{q}, \end{aligned} \tag{2}$$

where K_c is a positive constant and $||\cdot||$ denotes the Euclidean 2-norm.

To facilitate controller development, the following assumptions and lemmas are given first.

Assumption 1 The desired trajectory q_d is supposed to be known, bounded and twice differential, which implies that $\dot{q}_d, \ddot{q}_d$ exist.

Assumption 2 The lumped system uncertainty d_0 is assumed to be bounded and differentiable, yet the knowledge of its upper bound is unknown in prior.

Lemma 1 *[38] If there exists a continuously differentiable positive definite function: $V(x) : U \to \mathcal{R}$ satisfying the following inequality,*

$$\dot{V}(x) \le -\alpha V(x) - \beta V^{\gamma}(x), t_{\gamma} \ge t_0, V(x_0) \ge 0, \tag{3}$$

where U is a domain $U \in \mathcal{R}^n$ that contains the origin $x = 0$ and $\alpha, \beta > 0, 0 < \gamma < 1$ are constants, then the equilibrium point $x = 0$ is exponential stable with the settle time

$$t_{\gamma} \le \frac{1}{\alpha(1-\gamma)} \ln \frac{\alpha V^{1-\gamma}(x_0) + \beta}{\beta}, \tag{4}$$

where x_0 is any given initial states.

According to Lemma 1, the sliding mode surface and estimated errors will be proved to be finite-time convergent in next section.

Plant: Defining system states as $q_1 = q, q_2 = \dot{q}$ for convenience, then the system (1) is reformed as

$$\begin{cases} \dot{q}_1 = q_2, \\ \dot{q}_2 = f(q_1, q_2) + \tau + d_1, \end{cases} \tag{5}$$

where $f(q_1,q_2) = -M^{-1}(q_1)C(q_1,q_2)q_2$, $d_1 = M^{-1}(q_1)d_0$, and $\tau = M^{-1}(q_1)(u - G(q_1))$ is an additional controller designed in the next section.

Submit tracking errors $e_1 \triangleq q_1 - q_d, e_2 \triangleq q_2 - \dot{q}_d$ into the system model (5), one gets,

$$\begin{cases} \dot{e}_1 = e_2, \\ \dot{e}_2 = f(q_1,q_2) + \tau - \ddot{q}_d + d_1. \end{cases} \tag{6}$$

Target: This paper is dedicated to constructing an observer-based continuous adaptive SMC $\tau = \tau(t, q, q_d, \dot{q}_d, \ddot{q}_d)$ for the plant (6) in the presence of system uncertainties without knowledge of its upper bound in prior, such that system states can track the desired trajectories.

Notation 1: A matrix $K > 0$ represents the matrix is positive definite, and

$$\lambda_{min}(K) I_n \le K \le \lambda_{max}(K) I_n, \tag{7}$$

in which $\lambda_{min}(\cdot), \lambda_{max}(\cdot)$ denote the minimal and maximal eigenvalues of K, respectively.

Notation 2: For convenience, we denote $x^{[a]} = |x|^a \mathrm{sign}(x)$, where $\mathrm{sign}(\cdot)$ is the sign function.

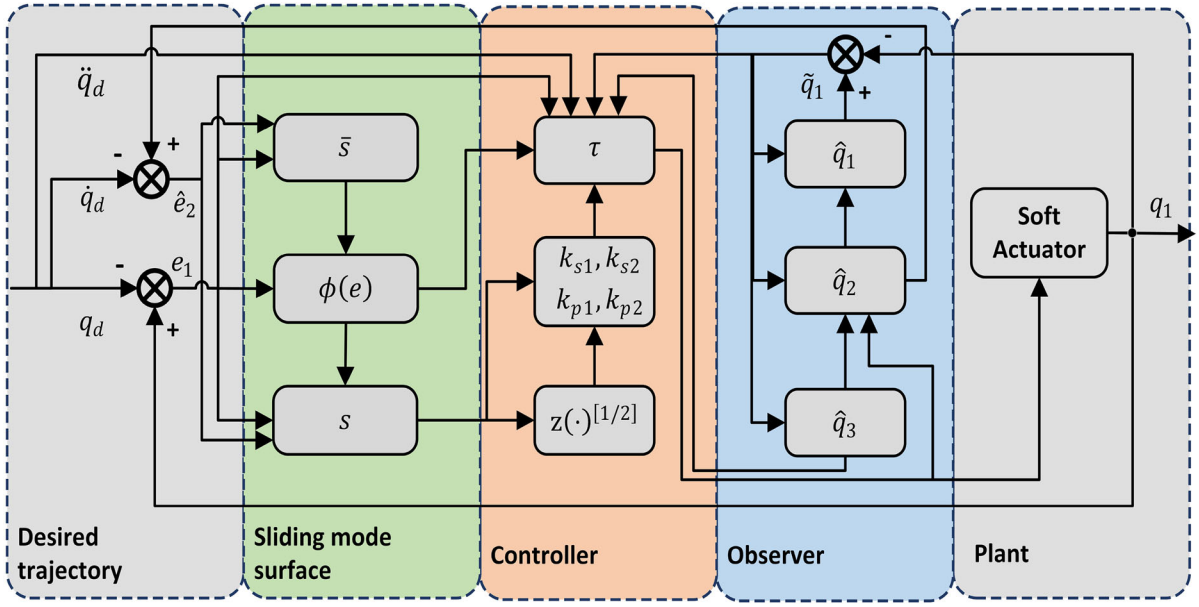

Fig. 1 The proposed observer-based continuous adaptive SMC scheme

3 Observer-based continuous adaptive SMC scheme

To achieve control target, the proposed observer-based SMC scheme mainly consists of a high-order sliding mode (HOSM) observer, an NFTSM and an STC as illustrated in Fig. 1. First, the HOSM-based observer is utilized to estimate unmeasurable states and further construct a continuous controller. Second, an NFTSM is employed for the finite-time stability of system states on the surface, the nonsingularity of control inputs and the robustness of the closed-loop system. Finally, an adaptive controller is achieved by the STA.

3.1 Observer utilization

The HOSM-based observer is [29]

$$\begin{cases} \dot{\hat{q}}_1 = -k_{11}(q_1 - \hat{q}_1)^{[\frac{2}{3}]} - k_{12}(q_1 - \hat{q}_1) + \hat{q}_2, \\ \dot{\hat{q}}_2 = -k_{21}(q_1 - \hat{q}_1)^{[\frac{1}{2}]} - k_{22}(q_1 - \hat{q}_1) \\ \qquad\quad + f\left(q_1, \hat{q}_2\right) + \tau + \hat{q}_3, \\ \dot{\hat{q}}_3 = -k_{31}\text{sign}(q_1 - \hat{q}_1), \end{cases} \tag{8}$$

where $\hat{q}_1$, $\hat{q}_2$ and $\hat{q}_3$ are the estimation of angle q_1, velocity q_2 and system uncertainties, respectively. k_{11}, k_{12}, k_{21}, k_{22}, k_{31} are positive-definite diagonal matrices. Noticing that the right-hand side of the above equations is discontinuous, thus it means the Filippov's solution in this paper.

Defining estimated errors as $\tilde{q}_1 = \hat{q}_1 - q_1, \tilde{q}_2 = \hat{q}_2 - q_2, \tilde{q}_3 = \hat{q}_3 - d_1$, then the model (8) is rewritten as

$$\begin{cases} \dot{\tilde{q}}_1 = -k_{11}\tilde{q}_1^{[\frac{2}{3}]} - k_{12}\tilde{q}_1 + \tilde{q}_2, \\ \dot{\tilde{q}}_2 = -k_{21}\tilde{q}_1^{[\frac{1}{2}]} - k_{22}\tilde{q}_1 + \tilde{q}_3 + d_2, \\ \dot{\tilde{q}}_3 = -k_{31}\text{sign}(\tilde{q}), \end{cases} \tag{9}$$

where $d_2 = f(q_1, \hat{q}_2) - f(q_1, q_2) + d_1$ is a bounded lumped uncertainties according to Assumption 2. The estimated errors (9) have been proved to be finite-time convergent in previous works [29,39–41], and the proof is omitted here for clarity.

3.2 Controller design

Inspired by [34,35,42], the sliding mode surface is selected as

$$s = \hat{e}_2 + \lambda_{11}e_1 + \lambda_{12}\phi(e_1), \tag{10}$$

where $\hat{e}_2 = \hat{q}_2 - \dot{q}_d$ is an estimated tracking error, $\lambda_{11}, \lambda_{12}$ are positive constants, and

$$\phi(e_1) = \begin{cases} e_1^{[a]}, & \text{if } \ \bar{s} = 0, \\ e_1^{[a]}, & \text{if } \ \bar{s} \neq 0 \cap |e_1| \geq \sigma, \\ \mu_1 e_1 + \mu_2 e_1^{[b]}, & \text{if } \ \bar{s} \neq 0 \cap |e_1| < \sigma, \end{cases} \tag{11}$$

in which $\bar{s} = \hat{e}_2 + \lambda_{13}e_1 + \lambda_{14}e_1^{[b_2]}$, $\frac{1}{2} < a < 1, 1 < b < 2, 0 < b_2 < 1, \mu_1 > 0, \mu_2 > 0, \sigma > 0$. Therefore, the time derivative of $\phi(e_1)$ is

$$\dot{\phi}(e_1) = \begin{cases} a|e_1|^{a-1}\dot{e}_1, & \text{if } \bar{s} = 0 \\ a|e_1|^{a-1}\dot{e}_1, & \text{if } \bar{s} \neq 0 \cap |e_1| \geq \sigma \\ \mu_1\dot{e}_1 + \mu_2 b|e_1|^{b-1}\dot{e}_1, & \text{if } \bar{s} \neq 0 \cap |e_1| < \sigma \end{cases}$$
$$= \begin{cases} a|e_1|^{a-1}(\hat{q}_2 - \tilde{q}_2), & \text{if } \bar{s} = 0, \\ a|e_1|^{a-1}(\hat{q}_2 - \tilde{q}_2), & \text{if } \bar{s} \neq 0 \cap |e_1| \geq \sigma, \\ (\mu_1 + \mu_2 b|e_1|^{b-1})(\hat{q}_2 - \tilde{q}_2), & \text{if } \bar{s} \neq 0 \cap |e_1| < \sigma. \end{cases} \tag{12}$$

According to the sliding mode surface definition (10), $s, \dot{s}$ are continuous if and only if the following conditions are satisfied,

$$\begin{cases} \sigma^{[a]} = \mu_1\sigma + \mu_2\sigma^{[b]}, \\ a\,|\sigma|^{a-1} = \mu_1 + \mu_2 b\,|\sigma|^{b-1}. \end{cases} \tag{13}$$

Therefore, one has

$$\begin{cases} \mu_1 = \frac{b-a}{b-1}\sigma^{a-1}, \\ \mu_2 = \frac{a-1}{b-1}\sigma^{a-b}. \end{cases} \tag{14}$$

The continuity of s and $\dot{s}$ is a necessary condition for the construction of a continuous controller.

Theorem 1 *Consider the system (6) with Assumptions 1 and 2. The control target will be achieved if the controller τ is constructed as*

$$\begin{aligned} \tau = {} & k_{21}\tilde{q}_1^{[\frac{1}{2}]} + k_{22}\tilde{q}_1 - f\left(q_1, \hat{q}_2\right) - \hat{q}_3 \\ & + \ddot{q}_d - \lambda_{11}\hat{e}_2 - \lambda_{12}\phi_1(e_1) \\ & - k_{s1}s^{[\frac{1}{2}]} - k_{s2}s - \int_0^t k_{p1}sign\,(s) - k_{p2}s dt_\sigma, \end{aligned} \tag{15}$$

where the sliding surface s is defined as (10), and

$$\phi_1(e_1) = \begin{cases} a|e_1|^{a-1}\hat{q}_2, & \text{if } \bar{s} = 0, \\ a|e_1|^{a-1}\hat{q}_2, & \text{if } \bar{s} \neq 0 \cap |e_1| \geq \sigma, \\ (\mu_1 + \mu_2 b|e_1|^{b-1})\hat{q}_2, & \text{if } \bar{s} \neq 0 \cap |e_1| < \sigma. \end{cases} \tag{16}$$

The controller gains $k_{s1}, k_{s2}, k_{p1}, k_{p2}$ are updated by

$$\begin{cases} k_{s1} = k_{z1}\sqrt{z}, k_{s2} = k_{z2}z, \\ k_{p1} = k_{z3}z, k_{p2} = k_{z4}z^2, \\ \dot{z} = k_{zu}s^{[\frac{1}{2}]}, \end{cases} \tag{17}$$

where k_{zu} is a positive constant, and $k_{z1}, k_{z2}, k_{z3}, k_{z4}$ should be properly selected to satisfy

$$-9k_{z1}^2k_{z3}^2 - 8k_{z2}k_{z3}^2 + 16k_{z2}k_{z4} > 0. \tag{18}$$

Proof The time derivative of s along the tracking error system (6) is

$$\begin{aligned} \dot{s} &= \dot{\hat{e}}_2 + \lambda_{11}\dot{e}_1 + \lambda_{12}\dot{\phi}(e_1) \\ &= \dot{\hat{q}}_2 - \ddot{q}_d + \lambda_{11}e_2 + \lambda_{12}d_m + \lambda_{12}\dot{\phi}(e_1) \\ &= -k_{21}|\tilde{q}|^p\text{sign}(\tilde{q}_1) - k_{22}\tilde{q}_1 + f\left(q_1, \hat{q}_2\right) \\ &\quad + \tau + \hat{q}_3 - \ddot{q}_d + \lambda_{11}e_2 + \lambda_{12}d_m + \lambda_{12}\dot{\phi}(e_1) \\ &= -k_{s1}s^{[\frac{1}{2}]} - k_{s2}s \\ &\quad - \int_0^t k_{p1}\text{sign}\,(s) - k_{p2}s dt_\sigma + d_3, \end{aligned} \tag{19}$$

where $d_3 = -\lambda_{11}\tilde{q}_2 + \tilde{q}_3 + \lambda_2 d_2$ is differentiable, and there exists an unknown positive constant D, such that $|d_3| < D$ under Assumption 2. Therefore, the equation (19) can be rewritten as

$$\begin{cases} \dot{s} = -k_{s1}s^{[\frac{1}{2}]} - k_{s2}s + \xi, \\ \dot{\xi} = -k_{p1}\text{sign}\,(s) - k_{p2}s + \dot{d}_3, \end{cases} \tag{20}$$

where ξ is an auxiliary state. The finite-time stability of the improved STA system (20) is proved in Appendix A for brevity. Therefore, the sliding mode surface is reached in finite time, i.e., $s(t) = 0, t > t_s$, where t_s is the reaching time. Further, the system is then enforced on the sliding surface in the rest of time since $\dot{s}s < 0, \forall s \neq 0$.

As introduced in Subsection 3.1, the estimated errors also converge to zero in finite time, and hence, $\hat{e}_2$ converges to e_2 in finite time. Therefore, on the sliding phase, the system is divided into three cases according to the range of $\bar{s}$.

Case 1: $\bar{s} = e_2 + \lambda_{21}e_1 + \lambda_{22}e_1^{[b_2]} = 0, 0 < b_2 < 1$, which induces that the tracking error converges to zero in finite time.

Case 2: $\bar{s} \neq 0 \cap |e_1| \geq \sigma$, then $s = e_2 + \lambda_{11}e_1 + \lambda_{12}e_1^{[a]} = 0, \frac{1}{2} < a < 1$, which is also a fast terminal sliding mode surface, and the tracking error converges to zero in finite time.

Case 3: $\bar{s} \neq 0 \cap |e_1| < \sigma$, then $s = e_2 + \lambda_{11}e_1 + \lambda_{12}\mu_1 e_1 + \lambda_{12}\mu_2 e_1^{[b]} = 0, 1 < b < 2$, and the tracking error asymptotically converges to zero as time tends to infinite. However, it should be noted that $|e_1| < \sigma$ in this case, where σ is an arbitrary small positive constant, and thus, the tracking error can be arbitrarily small.

This completes the proof. □

Remark 1 As illustrated in the proof, the estimated error system and the tracking error system are both

finite-time stable, i.e., the separation principle is satisfied, which enables us to design the observer and the tracking control law separately [43,44].

Remark 2 Compared with the conventional STA, which either does not contain or only has one damping term $k_{s2}s$ [45], the improved STA (9) contains two damping terms $k_{s2}s$, $k_{p2}s$ to take a shorter convergence time and reduce the overestimation of error. As proved in Appendix A, the extended damping term $k_{p2} = k_{z4}z^2$ is significantly important to guarantee the positive definite matrices A_4, A_5, which is one of the key steps of the proof.

Remark 3 The initial gains of the controller are properly chosen to satisfy the condition (18), while they will increase adaptively according to the uncertainties bound since the updated law is always positive except $s = 0$ in (17). However, s may not exactly be zero due to communication delays and measurement noises in practice. The boundary layer technical can be used to limit the updated law, i.e.,

$$\dot{z} = \begin{cases} k_{zu}s^{[\frac{1}{2}]}, & \text{if} \quad |s| > \sigma_s, \\ 0, & \text{if} \quad |s| \le \sigma_s, \end{cases} \tag{21}$$

where σ_s is a positive constant.

Remark 4 The proposed control scheme consists of a HOSM-based observer (8), an STA-based controller (15) and an NFTSM (10). The observer is followed by the previous work [29], and thus, the effect of the parameters on the performance of the closed-loop system is similar. For example, increasing damping gains k_{12}, k_{22} reduces overshoot and settle time, while it also increases the risk of saturation controllers. For the controller, damping gains k_{12}, k_{22} are a trade-off between dynamic performances and saturation risks, and other parameters should satisfy the condition (18) to guarantee finite-time stability. For the sliding mode surface, a smaller σ may bring in higher control precision as indicated by (10) and (11). However, we can know from (12) that an inappropriately small σ will drive the system trajectory near the singularity point and result in the degradation of the dynamic performances. For the NFTSM, $\lambda_{13}, \lambda_{14}$ are related to the settle time of tracking errors on the terminal sliding mode surface $\bar{s}$ according to the finite-time stability lemma. Similarly, $\lambda_{13}, \lambda_{14}, \mu_1, \mu_2$ make similarly effects on the surface s. With above observations, the feedback gains of the proposed controller can be suitably chosen after trial-in-errors in the following simulations and experiments.

4 Discussion of control scheme

Compared with relevant control schemes, the proposed scheme characterizes as continuity, singularity-free, faster convergence rate and higher tracking accuracy.

4.1 Continuity

The improved STA can be also utilized as an observer for the system (6), which takes a form as

$$\begin{cases} \dot{\hat{q}}_1 = -k_{1a}\tilde{q}^{[\frac{1}{2}]} - k_{1b}\tilde{q} + \hat{q}_2, \\ \dot{\hat{q}}_2 = -k_{1c}\text{sign}(\tilde{q}) - k_{1d}\tilde{q} + f\left(q_1, \hat{q}_2\right) + \tau_1. \end{cases} \tag{22}$$

Moreover, a LSM is chosen as

$$s_1 = \hat{e}_2 + \lambda_1 e_1. \tag{23}$$

Therefore, the time derivative of s_1 is

$$\begin{aligned} \dot{s}_1 &= \dot{\hat{e}}_2 + \lambda_1 \dot{e}_1 = \dot{\hat{e}}_2 + \lambda_1 e_2 \\ &= \dot{\hat{q}}_2 - \ddot{q}_d + \lambda_1 \tilde{q}_2 + \lambda_1 \hat{e}_2 \\ &= k_{1c}\text{sign}\left(\tilde{q}_1\right) + k_{1d}\left(\tilde{q}_1\right) + f\left(q_1, \hat{q}_2\right) \\ &\quad + \tau_1 - \ddot{q}_d + \lambda_1 \tilde{q}_2 + \lambda_1 \hat{e}_2. \end{aligned} \tag{24}$$

If the controller τ_1 is constructed as

$$\begin{aligned} \tau_1 = &-f\left(q_1, \hat{q}_2\right) + \ddot{q}_d - \lambda_1 \hat{e}_2 - k_{1c}\text{sign}\left(\tilde{q}_1\right) \\ &-k_{1d}\tilde{q}_1 - k_{1e}s_1^{[1/2]} - k_{1f}s_1 \\ &- \int_0^t k_{1g}\text{sign}\left(s_1\right) + k_{1h}s_1 d\sigma \\ &- \int_0^t -\lambda_1 k_{1c}\text{sign}\left(\tilde{q}_1\right) - \lambda_1 k_{1d}\tilde{q}_1 d\sigma, \end{aligned} \tag{25}$$

and submitting the controller (25) into (24), then

$$\begin{cases} \dot{s}_1 = -k_{1e}s_1^{[\frac{1}{2}]} - k_{1f}s_1 + \xi_1, \\ \dot{\xi}_1 = -k_{1g}\text{sign}\left(s_1\right) - k_{1h}s_1 \\ \qquad + \lambda_1 k_{21}\text{sign}\left(\tilde{q}_1\right) + \lambda_1 k_{22}\tilde{q}_1 d\sigma + \lambda_1 \dot{\tilde{q}}_2 \\ \quad = -k_{1g}\text{sign}\left(s_1\right) - k_{1h}s_1 + \lambda_1 \dot{d}_2, \end{cases} \tag{26}$$

where ξ_1 is an auxiliary state.

Consequently, the plant is converted into an improved STA scheme, but the controller (25) is discontinuous since it contains the term $k_{1c}\text{sign}(\tilde{q}_1)$. By exploiting the HOSM observer (8), the proposed controller (15) is continuous.

4.2 Singularity-free

To achieve a faster convergence rate on the sliding mode surface as well as a continuity controller, a finite-time

convergent FTSM surface is developed for the system (6)

$$s_2 = \hat{e}_2 + \lambda_{21} e_1 + \lambda_{22} e_1^{a_2}, \tag{27}$$

where $\lambda_{21}, \lambda_{22} > 0, 0 < a_2 < 1$ are constants, and the velocity is estimated by HOSM-based observer (8).

Therefore, the time derivative of s_2 is

$$\begin{aligned}
\dot{s}_2 &= \dot{\hat{e}}_2 + \lambda_{21}\dot{e}_1 + a\lambda_2 \dot{e}_1^{a_2-1} \\
&= \dot{\hat{e}}_2 + \lambda_{21} e_2 + a\lambda_2 e_2^{a_2-1} \\
&= \dot{\hat{q}}_2 - \ddot{q}_d + \lambda_{21}\tilde{q}_2 + \lambda_{21}\hat{e}_2 \\
&\quad + a_2\lambda_{22}\tilde{q}_2^{a_2-1} + a_2\lambda_{22}\hat{e}_2^{a_2-1} \\
&= -k_{21}\tilde{q}_1^{[p]} - k_{22}\tilde{q}_1 + f\left(q_1, \hat{q}_2\right) - \ddot{q}_d \\
&\quad + \tau_2 + \lambda_{21}\hat{e}_2 + a_2\lambda_{22}\hat{e}_2^{a_2-1} \\
&\quad + \lambda_{21}\tilde{q}_2 + a_2\lambda_{22}\tilde{q}_2^{a_2-1}.
\end{aligned} \tag{28}$$

If the robust controller τ_2, instead of τ in (6), is constructed as

$$\begin{aligned}
\tau_2 &= k_{21}\tilde{q}_1^{[\frac{1}{2}]} + k_{22}\tilde{q}_1 - f\left(q_1, \hat{q}_2\right) + \ddot{q}_d \\
&\quad - \lambda_{21}\hat{e}_2 - a_2\lambda_{22}\hat{e}_2^{a_2-1} - k_{2e}s_2^{[\frac{1}{2}]} - k_{2f}\left(s_2\right) \\
&\quad - \int_0^t k_{2g}\mathrm{sign}\left(s_2\right) + k_{2h}s_2 d\sigma,
\end{aligned} \tag{29}$$

and submitting τ_2 into (28), then one gets

$$\begin{cases}
\dot{s}_2 = -k_{2e}s_2^{[\frac{1}{2}]} - k_{2f}s_2 + \xi_2, \\
\dot{\xi}_2 = -k_{2g}\mathrm{sign}(s_2) - k_{2h}s + \dot{d}_4,
\end{cases} \tag{30}$$

where ξ_2 is an auxiliary state; $d_4 = \lambda_{21}\tilde{q}_2 + a_2\lambda_{22}\tilde{q}_2^{a_2-1}$.

Therefore, the system is also converted into the STA scheme, but the controller τ_2 should contain a term $\hat{e}_2^{a_2-1}, 0 < a_2 < 1$, which induces the singular problem when $\hat{e}_2 = 0, e_1 \neq 0$. In contrast, the proposed control law (15) is nonsingular.

4.3 Robustness

An alternative method to deal with the singularity problem under the condition of finite-time convergence rate on the sliding mode surface, except the proposed controller, is to design a NFTSM as

$$s_3 = e_1 + \lambda_{31} e_1^{[a_3]} + \lambda_{32}\hat{e}_2^{[b_3]}, \tag{31}$$

where $\lambda_{31}, \lambda_{32} > 0, 1 < b_3 < 2, a_3 > b_3$ are constants, and the velocity is estimated by HOSM-based observer (8). Therefore, the time derivative of s_3 is

$$\begin{aligned}
\dot{s}_3 &= \dot{e}_1 + \lambda_{31}a_3|e_1|^{a_3-1}\dot{e}_1 + \lambda_{32}b_3|\hat{e}_2|^{b_3-1}\dot{\hat{e}}_2 \\
&= e_2\left(1 + \lambda_{31}a_3\left|e_1\right|^{a_3-1}\right) \\
&\quad + \lambda_{32}b_3|\hat{e}_2|^{b_3-1}\left(-k_{21}\tilde{q}_1^{[p]} - k_{22}\tilde{q}_1\right) \\
&\quad + \lambda_{32}b_3|\hat{e}_2|^{b_3-1}\left(f\left(q_1, \hat{q}_2\right) + \tau_3 + \hat{q}_3 - \ddot{q}_d\right),
\end{aligned} \tag{32}$$

where the controller τ_3 is constructed as

$$\begin{aligned}
\tau_3 &= k_{21}\tilde{q}_1^{[\frac{1}{2}]} + k_{22}\tilde{q}_1 - f\left(q_1, \hat{q}_2\right) - \hat{q}_3 + \ddot{q}_d \\
&\quad - \frac{1}{\lambda_{32}b_3}\hat{e}_2^{[2-b_3]}\left(1 + \lambda_{31}a_3\left|e_1\right|^{a_3-1}\right) \\
&\quad - k_{3g}s_3^{[\frac{1}{2}]} - k_{3h}s_3.
\end{aligned} \tag{33}$$

Submitting the controller (33) into (32), then

$$\begin{aligned}
\dot{s}_3 &= \lambda_{32}b_3|\hat{e}_2|^{b_3-1}\left(-k_{3g}s^{[\frac{1}{2}]} - k_{3h}s_3\right) \\
&\quad + \tilde{q}_2\left(1 + \lambda_{31}a_3\left|e_1\right|^{a_3-1}\right).
\end{aligned} \tag{34}$$

The stability of s_3 under controller (33) has been proved by the Lyapunov method [46]. Although the convergence rate on the sliding phase is guaranteed by the NFTSM, the convergence rate on the reaching phase is slowed down by the term $|\hat{e}_2|^{b_3-1}$, especially when $\hat{e}_2$ is small. For example, $\hat{e}_2 = 0.25, b_3 = 1.5$, and then, $|\hat{e}_2|^{b_3-1} = 0.5$. The prolonged reaching phase implies that the robustness of the controller is attenuated. Besides, the STA is difficult to be utilized on this sliding model surface for constructing adaptive-tuning controllers.

4.4 Tracking accuracy

If the HOSM-based observer (8) is employed with a LSM (23), the controller can be constructed as

$$\begin{aligned}
\tau_4 &= k_{21}\tilde{q}^{[\frac{1}{2}]} + k_{22}\tilde{q}_1 - f\left(q_1, \hat{q}_2\right) + \ddot{q}_d - \lambda_1\hat{e}_2 \\
&\quad - k_{4e}s_1^{[\frac{1}{2}]} - k_{4f}s_1 \\
&\quad - \int_0^t k_{4g}\mathrm{sign}\left(s_1\right) + k_{4h}s_1 d\sigma;
\end{aligned} \tag{35}$$

therefore, one gets the same structure as (30). It is noted that the singularity-free of τ_4 and convergence rate of s_1 can be both guaranteed, but the biggest problem is that the tracking error is asymptotically converged to zero, which means the error will not be zero in finite time.

The sliding mode surface (10) is inspired from previous works [34,35,42], but the tracking error converges

to a predefined manifold, not zero and controllers in previous works require the measurable velocity feedback. Thanks to the HOSM-based observer and STC, both estimated and tracking errors of the closed-loop system will either converge to zero or an arbitrary small manifold in finite time, and it will tend to zero thereafter.

Although an STA-based controller is continuous, the scheme consisted of an STA-based observer and an STA-based controller is discontinuous. Furthermore, system states on the LSM are asymptotically stable, whereas tracking errors cannot converge into zero in finite time. To achieve continuous inputs and finite-time stability, an HOSM-based observer and an FTSM are both utilized in the HOSM+FTSM scheme. However, the biggest challenge of the HOSM+FTSM lies in the singular problem. An NFTSM is applied to HOSM+NFTSM to eliminate the singular problem, but the convergence rate of the surface is slowed down by a feedback term, which implies that the robustness of the system is degraded. The contradiction between the singularity of FTSM and the degraded robustness of NFTSM is solved by a novel NFTSM, and thus, the proposed control scheme has nonsingularity and stronger robustness. Furthermore, the proposed scheme is also adaptive and continuous due to the STA-based controller and the HOSM-based observer. The above discussion is shown in Table 2.

5 Verification

5.1 Dynamic model

As illustrated in Fig. 2a, a pneumatic network actuator mainly consists of a bottom layer and a top layer. The bottom layer is smooth, flexible but inextensible due to an embedded inextensible layer (usually fabricated by paper). In contrast, the top layer is concave–convex, flexible and extensible attributing to deformable cavity chambers. If the internal pressure increases, the neighboring chambers will be inflated and squeezed into each other, but the bottom layer holds a constant length. Consequently, the pneumatic network actuator is bent to an angle as shown in Fig. 2b.

As shown in Fig. 2a, the total width, length and height of the pneumatic network actuator are denoted as W, L, H, respectively. In detail, W_1 is the width of the anterior wall. L_1, L_2, L_3 denote the length of the

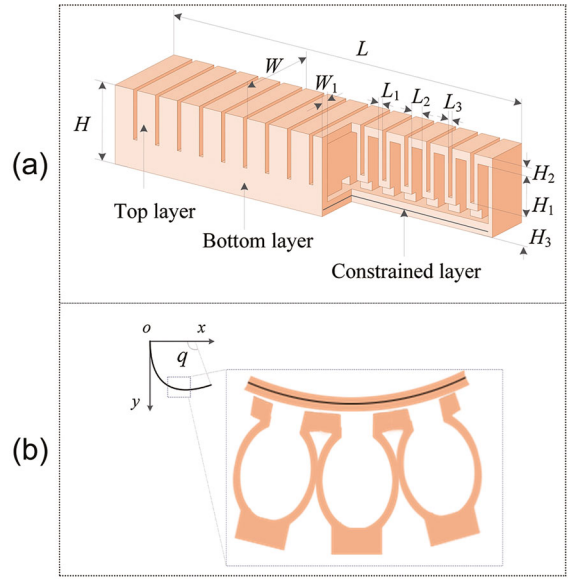

Fig. 2 A pneumatic network actuator with full structure parameters before and after inflating. **(a)** A schematic diagram of the initial state of a pneumatic network actuator with full geometrical parameters. **(b)** A pneumatic network actuator is vertically fixed as shown on the top-left with three zoomed-in inflated chambers. The fixed point, horizontal direction and vertical direction are set as the coordinate origin, x-axis and y-axis, respectively

exterior wall, the distance between two exterior walls of a chamber and the distance between exterior walls of neighboring chambers. H_1, H_2, H_3 are the height of the top wall, the exterior wall and the bottom layer, respectively.

Under the coordinate defined in Fig. 2b, the dynamic model of the pneumatic network actuator is addressed by exploring the Lagrangian method and Taylor expansions of sine and cosine functions [47],

$$M(q)\ddot{q} + C(q,\dot{q})\dot{q} + G_v(\dot{q}) = \tau + d_0, \tag{36}$$

where

$$\begin{aligned} M(q) &= mL^2\left(\frac{1}{20} - \frac{q^2}{504}\right), \\ C(q,\dot{q}) &= -\frac{mL^2 q\dot{q}}{504}, \\ G_v(q) &= \frac{mgLq}{12}, \\ \tau &= k_p p, \end{aligned}$$

and m, g are the mass and gravity coefficient, respectively. Since the pneumatic network actuator is actually driven by internal pressure p, the controller will

be eventually converted into the pressure with an estimated coefficient k_p [47]. It should note that the unmodeled dynamics and external disturbances are seemed as system uncertainties, which are contained in d_0.

5.2 Simulation

To verify the effectiveness, continuity, singularity-free, robustness and tracking accuracy, the proposed control scheme is compared with four other control schemes. For each control scheme, the related observer, sliding mode surface and controller are presented in Table 1. The gains of observers, sliding mode surfaces, controllers are selected after trials and errors, see Appendix B for details. In addition, the geometrical parameters of the simulated actuator are also omitted here and presented in Appendix B for brevity. The reference trajectory is set as $q_d = 0.9 + 0.8\sin(0.2t - \frac{\pi}{2})$ (rad), where the disturbance is $d_0 = \sin(t)$. Corresponding simulation results are, respectively, shown in Figs. 3–8.

5.2.1 Continuity and singularity-free

The continuity and singularity of comparative control inputs are illustrated in Fig. 3, and details are zoomed and shown in Fig. 4. As presented in Fig. 4a and b (the red curve), the continuity of STC is not achieved if the unavailable system states are estimated by STO, which accords with the description of the control scheme STO+LSM.

Although the HOSM+FTSM presents continuous inputs on the sliding phase, the singularity problem presents a high-gain oscillation phenomenon as presented in Fig. 3b. This problem is stepped from the singular term in the controller (29), which leads to a risk of the saturation controller and a great challenge for practical applications.

5.2.2 Robustness

Comparative sliding mode surfaces among different control schemes are shown in Fig. 5. All sliding mode surfaces can converge to zero in finite time. However, for the HOSM+NFTSM, the convergence time is significantly prolonged by the term of $|\hat{e}_2|^{b-1}$ as depicted in Fig. 5a (the black curve), where the reaching time is

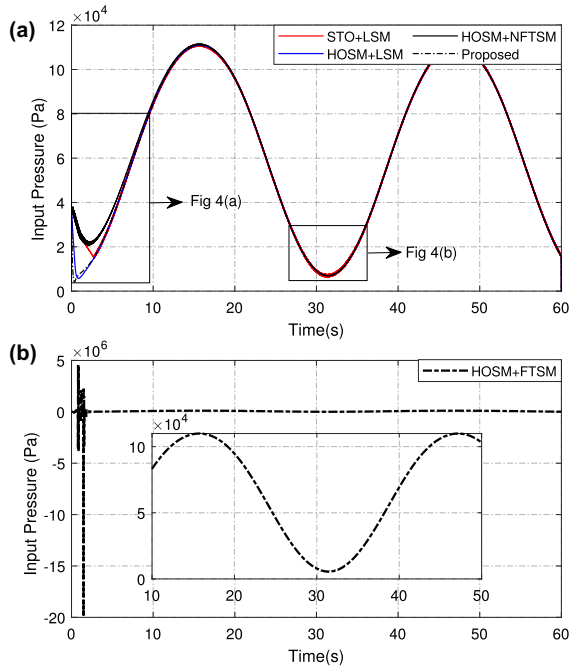

Fig. 3 Comparative control input pressure among the five control schemes

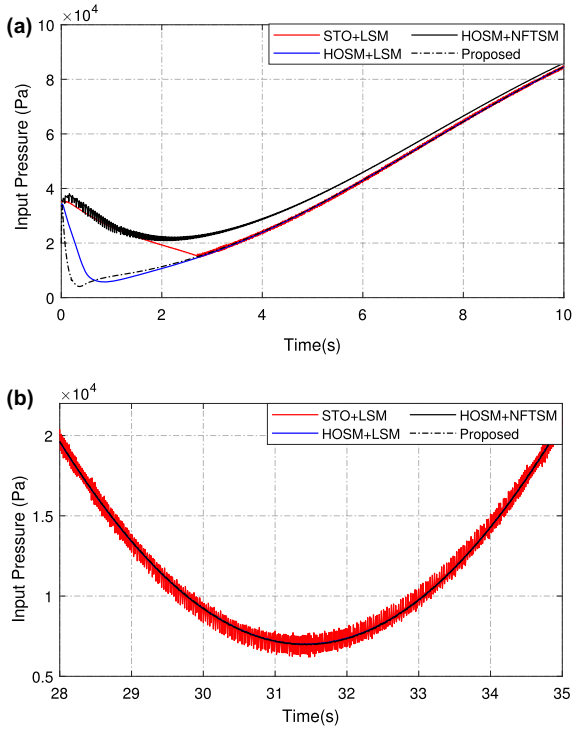

Fig. 4 The insets of input pressure at $t \in [0, 10]$ and $t \in [28, 35]$, respectively

Table 1 Comparative observers, sliding model surfaces and controllers

Name	Observer	Surface	Controller
STO+LSM	STO (22)	LSM (23)	STC (25)
HOSM+LSM	HOSM (8)	LSM (23)	STC (35)
HOSM+NFTSM	HOSM (8)	NFTSM (31)	STC (33)
HOSM+FTSM	HOSM (8)	FTSM (27)	STC (29)
Proposed	HOSM (8)	NFTSM (10)	STC (15)

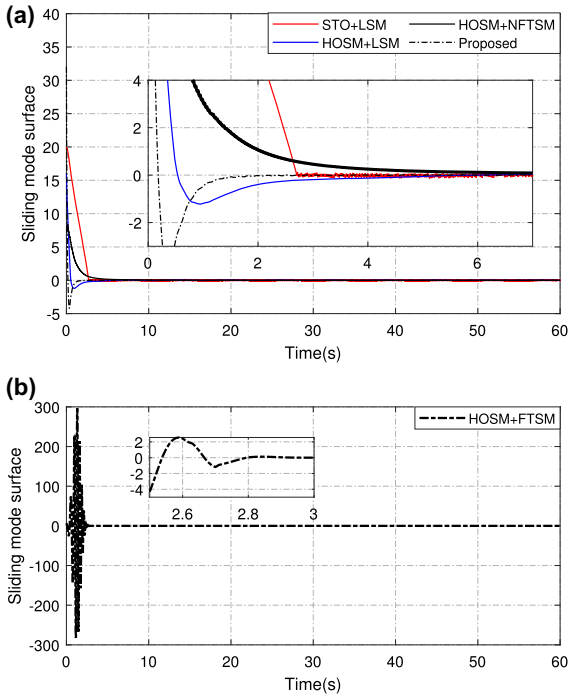

Fig. 5 The results of sliding mode surfaces

about 6.46s. The prolonged reaching phase implies that the control scheme HOSM+NFTSM posses weaker robustness than other schemes. In comparison, the proposed control scheme presents the shortest reaching phase to verify the strongest robustness. The reaching time of each control scheme is summarized in Table 2.

5.2.3 Tracking Accuracy

The root-mean-square error,

$$\text{RMSE} \triangleq \sqrt{\frac{1}{N}\sum_{i=1}^{N}(x_d(i)-x(i))^2}, \tag{37}$$

is utilized to compare tracking accuracy among these control results depicted in Figs. 6–8, where x_d, x are a desired and an actual value, respectively. According to the definition, a smaller RMSE implies a better tracking accuracy, or vice versa. As illustrated in Fig. 6, the control scheme HOSM+NFTSM has a slower convergence rate of sliding mode surface than other control schemes; meanwhile, its RMSE (3.32 degrees) is relatively large among these control strategies. As analyzed before, the term $|\hat{e}_2|^{b_2-1}$ in HOSM + NFTSM not only attenuates the system robustness but also enlarges the RMSE. Although the control scheme STO + LSM has a relatively smaller RMSE (2.87 degrees) than HOSM + NFTSM, its RMSE is still higher than other control schemes because of the chattering phenomenon shown in the inset of Fig. 6b (the red curve). Besides, the RMSE of the HOSM + LSM and the proposed scheme are 2.11 degrees and 0.96 degrees, respectively, because tracking errors under the HOSM + LSM are asymptotically convergent on the sliding phase. As separately described in Fig.7, the singularity problem of the HOSM+FTSM induces large tracking errors on the reaching phase. Although the problem is eliminated on the sliding phase, the RMSE is the largest (26.4 degrees) among the five control schemes.

Furthermore, the velocity can track the desired velocity under different controllers as presented in Fig. 8. The velocity is more easily to be contaminated by external disturbance compared with the bending angle as compared between Figs. 6 and 8. Therefore, the RMSEs of velocity tracking results under these controllers are bigger than bending angles. It should note that the control results under HOSM with FTSM also present the singularity problem, which leads to a huge RMSE, and they are omitted for brevity.

In conclusion, the related features of comparative control schemes are presented in Table 2. Thanks to the HOSM-based observer, the novel sliding mode sur-

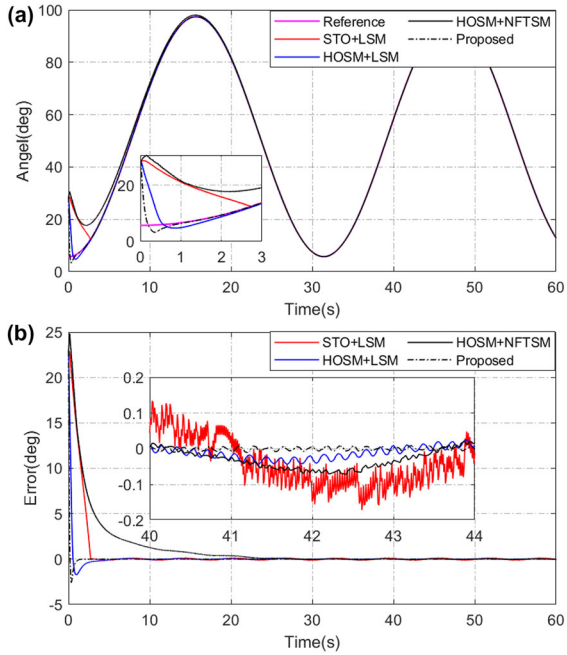

Fig. 6 Comparisons of position tracking control results between different controllers. (a) shows tracking control results under different controllers with a zoomed-in inset at $t \in [0, 3.5]$. (b) presents tracking errors, where an inset particularly shows errors at $t \in [40, 44]$

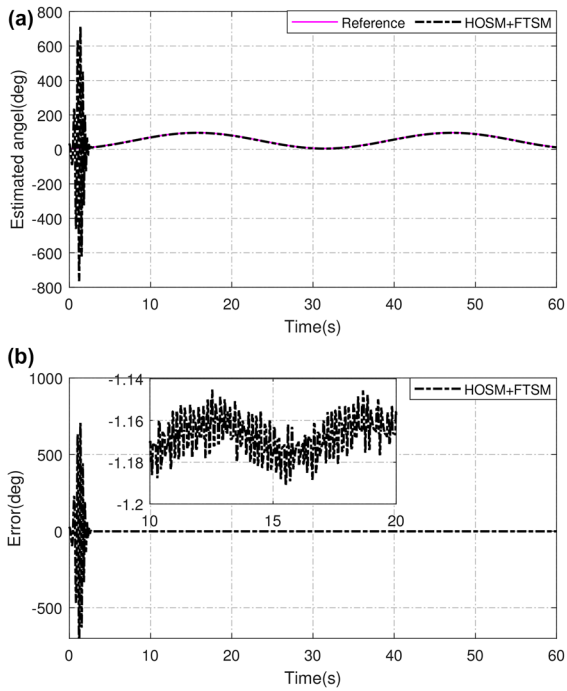

Fig. 7 The control results (a) and tracking errors (b) under HOSM with FTSM

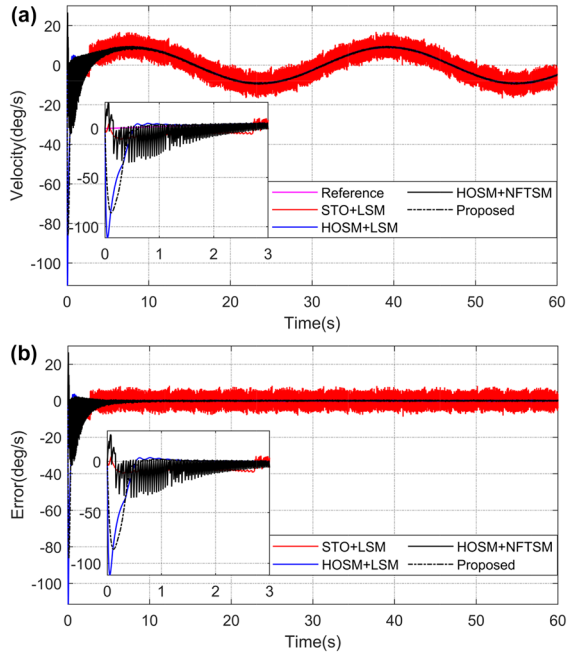

Fig. 8 Velocity control results and errors under different controllers

face and the STA-based controller, the proposed control scheme possesses better performances than comparative schemes.

5.3 Experiments

To further verify the proposed control scheme, an experimental platform is designed and set up as shown in Fig. 10. First, a pneumatic network actuator is fabricated by Ecoflex 00-30 (Smooth-on, Inc, USA) and vertically fixed on a metal framework. Second, a flex sensor (SpectraSymbol, Inc, USA) is calibrated by a high definition camera and the OpenCV toolbox of MATLAB. Finally, two solenoid valves (VT307, SMC, Inc, Japan) are utilized to control the air passages of the actuator, and a pressure sensor (MPX5500DP, Freescale Semiconductor, Inc, USA) measures the internal pressure. An air pump (KZP-PE, Kamoer, China) and an air cylinder are used to be a stable air source. Meantime, a host computer and an STM32 development board (mini F103, Xingyi, Inc, China) record the voltage change of the flex sensor.

Set the desired trajectory as $q_d = 0.8 - 0.4\cos(0.5t) - 0.4\exp(-0.5t)$(rad). Due to the singularity problem, the control scheme HOSM+FTSM is given up in the

Table 2 Comparative simulation results under different control schemes

Control scheme	Continuity	Singularity-free	Reaching time (s)	RMSE of angle (deg)	RMSE of velocity (deg/s)
STO+LSM	NO	YES	2.74	2.87	4.46
HOSM+LSM	YES	YES	3.42	2.11	4.13
HOSM+NFTSM	YES	YES	6.46	3.32	7.92
HOSM+FTSM	YES	NO	2.81	26.4	327.35
Proposed	**YES**	**YES**	**1.52**	**0.96**	**2.64**

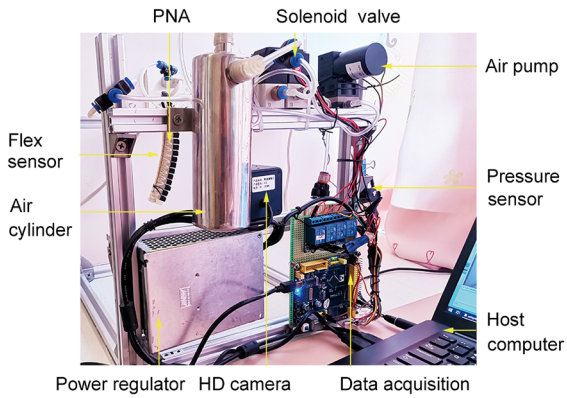

Fig. 9 The experiment platform

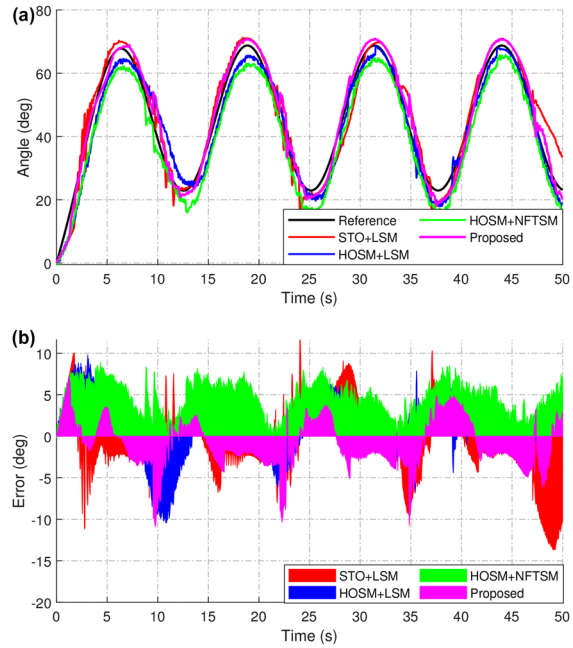

Fig. 10 The experiment results under four different control schemes

physical experiment for safety consideration, and gains of other control schemes are chosen after trial-in-errors and shown in Appendix B for brevity. Thereafter, experimental results are shown in Fig. 10. The slowest convergence rate of tracking errors among these controllers is HOSM + NFTSM, which presents the worst RMSE (6.32 degrees). Among these control results, the chattering phenomenon is significantly presented in the control scheme of STO+LSM (the red curve in Fig. 10a), and the RMSE is 4.43 degrees. The RMSE of HOSM+LSM is 4.039 degrees due to a slower convergence rate on the sliding surface, whereas the smallest RMSE is 3.169 degrees under the proposed control scheme.

The observer is validated by experimental results as presented in Figs. 11 and 12. (i) Figure 11 shows errors between actual angles and estimated angles in experiments. The control scheme HOSM+NFTSM (green line) presents bigger estimated errors than other schemes due to a slower convergence rate of sliding mode surface and weaker robustness of the closed-loop system. The STO+LSO (red line) shows a greater chattering phenomenon than other schemes due to the discontinuous control inputs. The HOSM+LSM (blue line) is smoother than STO+LSO and has smaller errors than HOSM+ NFTSM, but errors are slowly converged into zero due to the asymptotic stability of system states on the sliding mode surface. The proposed control scheme (magenta line) presents smaller errors and a faster convergence rate than other schemes. (ii) Due to unmeasurable velocity states in experiments, the actual velocity information is obtained by numerical differential on smoothed angles, and thus, estimated errors are presented in Fig. 12. Features of estimated velocity errors are basically identified with estimated angle errors, such as bigger errors of HOSM+NFTSM, greater chattering of STO+LSO. Since velocity is more

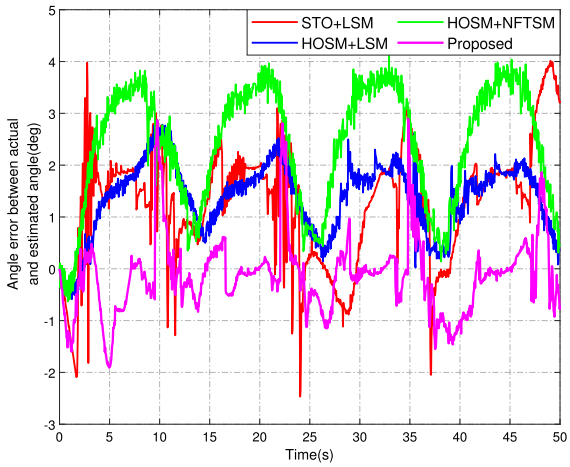

Fig. 11 Angle errors between actual and estimated results in experiments

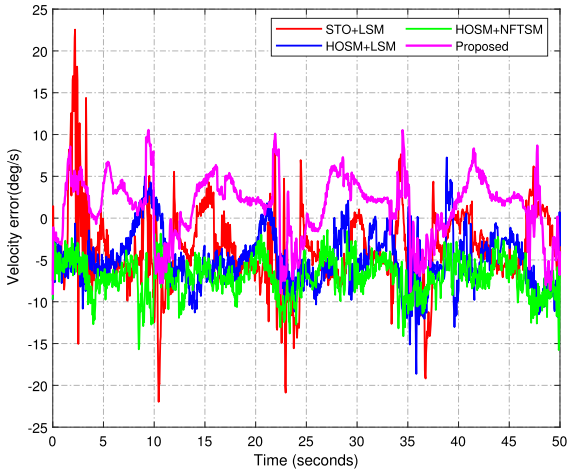

Fig. 12 Estimated velocity errors in experiments

sensitive to external noise than position, estimated errors of velocity are larger than the positions.

6 Conclusion and future work

This paper investigates a novel control scheme consisting of a HOSM-based observer, a nonsingular fast terminal sliding mode surface and an STA-based controller to solve the control challenge of soft actuators. By employing the observer, the unavailable system states are estimated to stress the continuity of SMC. The tracking errors of the closed-loop system are converged to zero or a predefined set in finite time and tend to zero thereafter under the proposed control scheme, which presents higher tracking accuracy than the relevant researches for soft actuators. The proposed controller is analyzed by the Lyapunov method and compared with other schemes. In the future, multi-soft actuators will be stabilized simultaneously for the applications of soft grippers and hands. Furthermore, a simple control schema with the same properties as the controller proposed is worth investigating for wider applications.

Acknowledgements This work was supported by the National Key Research and Development Project (No. 2020YFB1313701), the National Natural Science Foundation of China (No. 6160 3345, 62003309), the Outstanding Foreign Scientist Support Project of Henan Province (No. GZS2019008) and Science & Technology Research Project in Henan Province of China (No. 202102210098).

Author contributions No competing financial interest exists. Some or all data, models or code generated or used during the study are available from the corresponding author by request.

Appendix A

According to the update law (17) and (20), some auxiliary variances are defined as

$$\rho_1 = \sqrt{z}s^{[\frac{1}{2}]}, \rho_2 = s, \rho_3 = \xi. \tag{38}$$

Therefore,

$$\begin{aligned} &\frac{z}{|\rho_1|}\rho_1\rho_2 = \zeta\rho_1\rho_1, \frac{z}{|\rho_1|}\rho_2\rho_2 = z\rho_1\rho_2, \\ &\frac{z}{|\rho_1|}\rho_2\rho_3 = z\rho_1\rho_3, \end{aligned} \tag{39}$$

and

$$\begin{aligned} \dot{\rho} \triangleq \begin{bmatrix} \dot{\rho}_1 \\ \dot{\rho}_2 \\ \dot{\rho}_3 \end{bmatrix} &= -\frac{z}{2|\rho_1|}\underbrace{\begin{bmatrix} k_{z1} & k_{z2} & -1 \\ 0 & 0 & 0 \\ 2k_{z3} & 0 & 0 \end{bmatrix}}_{A_1}\begin{bmatrix} \rho_1 \\ \rho_2 \\ \rho_3 \end{bmatrix} \\ &\quad -\underbrace{\begin{bmatrix} 0 & 0 & 0 \\ zk_{z1} & zk_{z2} & -z \\ 0 & k_{z4}z & 0 \end{bmatrix}}_{A_2}\begin{bmatrix} \rho_1 \\ \rho_2 \\ \rho_3 \end{bmatrix} + \underbrace{\begin{bmatrix} \frac{\dot{z}}{2z}\rho_1 \\ \frac{\dot{z}}{z}\rho_2 \\ d_2 \end{bmatrix}}_{A_3} \\ &= -\frac{z}{2|\rho_1|}A_1\rho - A_2\rho + A_3. \end{aligned} \tag{40}$$

The candidate Lyapunov function is chosen as,

$$V_1 = \frac{1}{2}\rho^T P\rho, \tag{41}$$

where $P = \begin{bmatrix} 4k_{z3}+k_{z1}^2 & k_{z1}k_{z2} & -k_{z1} \\ k_{z1}k_{z2} & k_{z2}^2+4k_{z4} & -k_{z2} \\ -k_{z1} & -k_{z2} & 2 \end{bmatrix}$ is positive definite.

The derivative of V_1 with respect to time along with equations (40) is,

$$\begin{aligned}\dot{V}_1 &= -\frac{\zeta}{2\,|\rho_1|}\rho^T P A_1 \rho - \rho^T P A_2 \rho + \rho^T P A_3 \\ &= -\zeta\rho^T \begin{bmatrix} k_{z1}^2 k_{z2} & k_{z1}k_{z2}^2 + 2k_{z1}k_{z4} & -k_{z1}k_{z2} \\ * & k_{z2}\left(k_{z2}^2+4k_{z4}\right) & -k_{z2}^2-k_{z4} \\ * & * & k_{z2} \end{bmatrix}\rho \\ &\quad -\frac{\zeta}{2\,|\rho_1|}\rho^T \begin{bmatrix} k_{z1}^3+2k_{z3}k_{z1} & (k_{z1}^2+k_{z3})k_{z2} & -k_{z1}^2 \\ * & k_{z1}k_{z2}^2 & -k_{z1}k_{z2} \\ * & * & k_{z1} \end{bmatrix}\rho \\ &\quad +\frac{\dot{z}}{2z}\rho^T \underbrace{\begin{bmatrix} 4k_{z2}+k_{z1}^2 & \frac{3}{2}k_{z1}k_{z3} & -\frac{1}{2}k_{z1} \\ * & 2k_{z3}^2+8k_{z4} & -k_{z3} \\ * & * & 0 \end{bmatrix}}_{A_3'}\rho \\ &\quad \underbrace{-k_{z1}\rho_1 d_2 - k_{z2}\rho_2 d_2 + 2\rho_3 d_2}_{\Delta}. \end{aligned} \tag{42}$$

The time derivative of the V_1 is further equal to

$$\begin{aligned}\dot{V}_1 &= \frac{\dot{\zeta}}{2\zeta}\rho^T A_3'\rho + \Delta \\ &\quad -\frac{\zeta\rho^T}{2\,|\rho_1|}\underbrace{\begin{bmatrix} k_{z1}^3+2k_{z3}k_{z1} & 0 & -k_{z1}^2 \\ * & 5k_{z1}k_{z2}^2+8k_{z1}k_{z4} & -3k_{z1}k_{z2} \\ * & * & k_{z1} \end{bmatrix}}_{A_4}\rho \\ &\quad -\zeta\rho^T \underbrace{\begin{bmatrix} 2k_{z1}^2k_{z2}+k_{z3}k_{z2} & 0 & 0 \\ * & k_{z2}\left(k_{z2}^2+4k_{z4}\right) & -k_{z2}^2-k_{z4} \\ * & * & k_{z2} \end{bmatrix}}_{A_5}\rho \\ &= -\frac{\zeta}{2\,|\rho_1|}\rho^T A_4\rho - \zeta\rho^T A_5\rho + \frac{\dot{\zeta}}{2\zeta}\rho^T A_3'\rho + \Delta. \end{aligned} \tag{43}$$

The * in the matrices A_4 and A_5 denotes the symmetrical term of the matrix. The matrices A_4 and A_5 are positive definite if the inequality (18) holds. Further, noticing that the following inequalities are satisfied,

$$\begin{aligned} &\lambda_{min}\{A_3'\}||\rho||^2 \le \rho^T A_3'\rho \le \lambda_{max}\{A_3'\}||\rho||^2, \\ &\lambda_{min}\{A_4\}||\rho||^2 \le \rho^T A_4\rho \le \lambda_{max}\{A_4\}||\rho||^2, \\ &\lambda_{min}\{A_5\}||\rho||^2 \le \rho^T A_5\rho \le \lambda_{max}\{A_5\}||\rho||^2, \\ &\lambda_{min}\{P_a\}||\rho||^2 \le V_1 \le \lambda_{max}\{P_a\}||\rho||^2, \end{aligned} \tag{44}$$

The derivative of the Lyapunov function V_1 is

$$\begin{aligned}\dot{V}_1 &= -\frac{z}{2\,|\rho_1|}\rho^T A_4\rho - \rho^T A_5\rho + \frac{\dot{z}}{2z}\rho^T A_3'\rho + \Delta \\ &\le -\frac{z}{2\,|\rho_1|}\rho^T A_4\rho - \rho^T A_5\rho + \frac{\dot{z}}{2z}\lambda_{max}\{A_3'\}\rho^T\rho \\ &\quad +\sqrt{k_{z1}^2+k_{z2}^2+4D}||\rho|| \\ &\le -\frac{z}{2\,|\rho_1|}\lambda_{min}\{A_4\}\rho^T\rho - \lambda_{min}\{A_5\}\rho^T\rho \\ &\quad +\frac{\dot{z}}{2z}\lambda_{max}\{A_3'\}\rho^T\rho + \sqrt{k_{z1}^2+k_{z2}^2+4D}||\rho||. \end{aligned} \tag{45}$$

The time derivative of the V_1 is further equal to

$$\begin{aligned}\dot{V}_1 &\le -\frac{z}{2|\rho_1|}\lambda_{min}\{A_4\}||\rho||^2 + \sqrt{k_{z1}^2+k_{z2}^2+4D}||\rho|| \\ &\quad -\lambda_{min}\{A_5\}||\rho||^2 + \frac{\dot{z}}{2z}\lambda_{max}\{A_3'\}||\rho||^2. \end{aligned} \tag{46}$$

In virtue of the well-known inequality $(\rho_1^2+\rho_2^2+\rho_3^2)^{\frac{1}{2}} \le (|\rho_1|+|\rho_2|+|\rho_3|)$, $||\rho||^2 \ge ||\rho_1||^2$, $\rho^T\rho \le \frac{2}{\lambda_{min}(P_a)}V_1$, $-\rho^T\rho \le -\frac{2}{\lambda_{max}(P_a)}V_1$, then the derivative satisfies

$$\begin{aligned}\dot{V}_1 &\le -\left[\frac{2\lambda_{min}\{A_5\}}{\lambda_{max}(P_a)} - \frac{\dot{z}\,|\lambda_{max}\{A_3'\}|}{z\lambda_{min}(P_a)}\right]V_1 \\ &\quad -\left[\frac{z}{2}\lambda_{min}\{A_4\} - \sqrt{k_{z1}^2+k_{z2}^2+4D}\right] \\ &\quad \times\sqrt{\frac{2}{\lambda_{max}(P_a)}}V_1^{1/2}. \end{aligned} \tag{47}$$

Based on the update law $\dot{z} \ge 0$, then z is increased all the time except when $\tilde{q}_1 = 0$, so $\varphi_1 = \frac{2\lambda_{min}\{A_5\}}{\lambda_{max}(P_a)} - \frac{\dot{z}\,|\lambda_{max}\{A_3'\}|}{z\lambda_{min}(P_a)}$ and $\varphi_2 = \frac{z}{2}\lambda_{min}\{A_4\} - \sqrt{k_{z1}^2+k_{z2}^2+4D}$ will be positive in a short adjusting time. Then, $\dot{V}_1 \le -\varphi_1 V_1 - \varphi_2 V_1^{1/2}$. According to Lemma.1, the estimated errors converge to zero in finite time,

$$t_s \le \frac{2}{\varphi_1}\ln\frac{\varphi_1 V_1^{1/2}(x_0)+\varphi_2}{\varphi_2}. \tag{48}$$

This completes the proof. □

Appendix B

As discussed before, soft actuators are widely used as soft gloves. To mimic a human middle finger, the details of the simulated actuator are $W = 1.5\times10^{-2}$m, $L_1 = 8\times10^{-3}$m, $W_1 = 3\times10^{-3}$m, $W_2 = 2\times$

10^{-3}m, $H_1 = 7 \times 10^{-3}$m, $H_3 = 1.1 \times 10^{-2}$m, $L_{20} = 2 \times 10^{-3}$m, $N = 14$, $k_p = 6.2 \times 10^{-7}$, $G = 2.387 \times 10^6$Pa, $m = 4 \times 10^{-2}$kg.

In numerical simulations, gains are introduced as follows. In the control scheme of STO+LSM, the gains of the STO (22) are $k_{1a} = 7, k_{1b} = 5, k_{1c} = 4, k_{1d} = 10$, the gain of the LSM (23) is $\lambda_1 = 50$, and the gains of the STC (25) $k_{1e} = k_{1ez}\sqrt{z}, k_{1f} = k_{11f}z, k_{1g} = k_{11g}z, k_{1h} = k_{11h}z^2$ are updated by $k_{1ez} = 1.8, k_{11f} = 3, k_{11g} = 0.05, k_{11h} = 2, k_{zu} = 0.5$.

In the control scheme of HOSM+LSM, the gains of the HOSM observer (8) are $k_{11} = 7, k_{12} = 20, k_{21} = 10, k_{22} = 50, k_{31} = 20$, and the gains of LSM (23) and the updated law of controller are same to the STO+LSM.

In the control scheme of HOSM+NFTSM, parameters of NFTSM (31) are $\lambda_{31} = 42, \lambda_{32} = 0.1$, and feedback gains of the STC (33) are $a_3 = 2, b_3 = 1.5, k_{3g} = 6, k_{3h} = 2$.

In the control scheme of HOSM+FTSM, the parameters of FTSM (27) are $\lambda_{21} = 14, \lambda_{22} = 2$, and the gains of STC (29) are updated by $k_{2e} = k_{02z}\sqrt{z}, k_{2f} = k_{02f}z, k_{2g} = k_{02g}z, k_{2h} = k_{02h}z^2$, where $k_{02z} = 1.8, k_{02f} = 3, k_{2g} = 0.05, k_{02h} = 2, k_{zu} = 0.5$.

In the proposed control scheme, the observer (8), parameters of the NFTSM (10) are $\lambda_{11} = 14, \lambda_{12} = 2, \mu_1 = 4, \mu_2 = 2, a = 0.75, b = 1.5, b_2 = 0.5$, and the gains of proposed controller (15) are $k_{s1} = k_{s01}\sqrt{z}, k_{s2} = k_{s02}z, k_{p1} = k_{p01}z, k_{p2} = k_{p02}z$, where $k_{s01} = 2, k_{s02} = 3, k_{p01} = 0.05, k_{p02} = 2, k_{zu} = 0.5$.

In experiments, gains are selected after trial-inerrors. In the control scheme of STO+LSM, the gains of the STO (22), the LSM (23) and the STC (25) are $k_{1a} = 4, k_{1b} = 7, k_{1c} = 4, k_{1d} = 6, \lambda_1 = 12, k_{1ez} = 0.6, k_{11f} = 2.1, k_{11g} = 0.03, k_{11h} = 1.2, k_{zu} = 0.3$. In the control scheme of HOSM+LSM, the gains of the HOSM observer (8) and the LSM (23) are $k_{11} = 3, k_{12} = 12, k_{21} = 5, k_{22} = 13, k_{31} = 0.5, \lambda_1 = 12$. In the control scheme of HOSM+NFTSM, parameters of NFTSM (31) are $\lambda_{31} = 9, \lambda_{32} = 0.08$, and feedback gains of the STC (33) are $a_3 = 1.8, b_3 = 1.5, k_{3g} = 4.5, k_{3h} = 2.3$. In the control scheme of HOSM+FTSM, parameters of FTSM (27) and STC (29) are $\lambda_{21} = 9, \lambda_{22} = 2, k_{02z} = 0.6, k_{02f} = 2.1, k_{2g} = 0.03, k_{02h} = 1.5, k_{zu} = 0.3$. In the proposed control scheme, the observer (8), parameters of the NFTSM (10) and the controller (15) are $\lambda_{11} = 11, \lambda_{12} = 2, \mu_1 = 3.5, \mu_2 = 2, a = 0.75, b = 1.5, b_2 = 0.5, k_{s01} = 0.8, k_{s02} = 2.5, k_{p01} = 0.05, k_{p02} = 3, k_{zu} = 0.3$.

References

1. Heung, K.H.L., Tong, R.K.Y., Lau, A.T.H., Li, Z.: Robotic glove with soft-elastic composite actuators for assisting activities of daily living. Soft Robot. **6**(2), 289–304 (2019)
2. Tang, Z.Q., Heung, H.L., Tong, K.Y., Li, Z.: Model-based online learning and adaptive control for a human-wearable soft robot integrated system. Int. J. Robot Res. **38**(9), 1–21 (2019)
3. Fang, J., Yuan, J., Wang, M., Xiao, L.: Novel accordion-inspired foldable pneumatic actuators for knee assistive devices. Soft Robot. **7**(1), 95–108 (2019)
4. Katzschmann, R.K., DelPreto, J., MacCurdy, R., Rus, D.: Exploration of underwater life with an acoustically controlled soft robotic fish. Sci. Robot. **3**(16), eaar3449 (2018)
5. Rus, D., Tolley, M.T.: Design, fabrication and control of soft robots. Nature **521**(7553), 467–475 (2015)
6. Thuruthel, T.G., Shih, B., Laschi, C., Tolley, M.T.: Soft robot perception using embedded soft sensors and recurrent neural networks. Sci. Robot. **4**(26), eaav1488 (2019)
7. Melingui, A., Lakhal, O., Daachi, B., Mbede, J.B., et al.: Adaptive neural network control of a compact bionic handling arm. IEEE-Asme T Mech. **20**(6), 2862–2875 (2015)
8. Fang, G., Wang, X., Wang, K., Kit-Hang, L., et al.: Vision-based online learning kinematic control for soft robots using local gaussian process regression. IEEE Robot. Autom. Lett. **4**(2), 1194–1201 (2019)
9. Thieffry, M., Kruszewski, A., Duriez, C., Guerra, T.M.: Control design for soft robots based on reduced-order model. IEEE Robot. Autom. Lett. **4**(1), 25–32 (2019)
10. Best, C.M., Rupert, L., Killpack, M.D.: Comparing model-based control methods for simultaneous stiffness and position control of inflatable soft robots. Int. J. Robot. Res. **3**(1), 1–24 (2020)
11. Chen, W., Xiong, C., Liu, C., Li, P.: Fabrication and dynamic modeling of bidirectional bending soft actuator integrated with optical waveguide curvature sensor. Soft Robot. **6**(4), 495–506 (2019)
12. Zolfagharian, A., Kaynak, A., Noshadi, A., Kouzani, A.Z.: System identification and robust tracking of a 3D printed soft actuator. Smart Mater. Struct. **28**(7), 075025–075036 (2019)
13. Khawwaf, J., Zheng, J.C., Wang, H., Man, Z.H.: Practical model-free robust estimation and control design for an underwater soft IPMC actuator. IET Control. Theory A **14**(11), 1508–1515 (2020)
14. Wang, Y., Ye, W., Zhang, Y., Lai, X.: Modeling and tracking control for soft robots of dielectric elastomer actuators. Control Theory Appl. **37**(4), 871–880 (2020)
15. Chalanga, A., Kamal, S., Fridman, L.M., Bandyopadhyay, B.: Implementation of super-twisting control: super-twisting and higher order sliding-mode observer-based approaches. IEEE T Ind. Electron. **63**(6), 3677–3685 (2016)
16. Wang, W., Lin, H., Yang, H., Liu, W., et al.: Second-order sliding mode-based direct torque control of variable-flux memory machine. IEEE Access **8**, 34981–34992 (2020)

17. Pati, A.K., Sahoo, N.C.: A super-twisting sliding mode observer for boost inverter-based hybrid photovoltaic-battery system control. T I Meas. Control. **4**(1), 1–16 (2020)
18. Cao, G., Xie, C., Liu, Y.: Observer-based adaptive sliding mode tracking control for soft bending actuators, Proc. 2020 Chinese Automation Congress (CAC), pp. 5789-5794
19. Han, Y., Kao, Y., Gao, C.: Robust sliding mode control for uncertain discrete singular systems with time-varying delays and external disturbances. Automatica **75**, 210–216 (2017)
20. Han, Y., Su, C.-Y., Kao, Y., Gao, C.: Non-fragile sliding mode control of discrete switched singular systems with time-varying delays. IET Control Theory A **14**(5), 726–737 (2020)
21. Zhen, Z., Yu, C., Jiang, S., Jiang, J.: Adaptive super-twisting control for automatic carrier landing of aircraft. IEEE Trans. Aerospace Electron. Syst. **56**(2), 984–997 (2020)
22. Zhao, Y., Zhang, F., Huang, P., Liu, X.: Impulsive super-twisting sliding mode control for space debris capturing via tethered space net robot. IEEE T Ind. Electron. **67**(8), 6874–6882 (2020)
23. Lochan, K., Singh, J.P., Roy, B.K., Subudhi, B.: Adaptive time-varying super-twisting global SMC for projective synchronisation of flexible manipulator. Nonlinear Dynam. **93**(4), 2071–2088 (2018)
24. Zheng, S., Niu, X., Peng, C.: Adaptive super-twisting-like sliding mode control with prescribed performance for robot manipulators. J. Mech. Med. Biol. **19**(8), 1940053–1940068 (2019)
25. Raj, K., Muthukumar, V., Singh, S.N., Lee, K.W.: Finite-time sliding mode and super-twisting control of fighter aircraft. Aerospace Sci. Technol. **82–83**, 487–498 (2018)
26. Chen, H., Song, S., Li, X.: Robust spacecraft attitude tracking control with integral terminal sliding mode surface considering input saturation. T I Meas. Control. **41**(2), 405–416 (2019)
27. Ge, P., Dou, X., Quan, X., Hu, Q.: Extended-state-observer-based distributed robust secondary voltage and frequency control for an autonomous microgrid. IEEE Trans. Sustain. Energy **11**(1), 195–205 (2020)
28. Wang, Y.Y., Zhang, R., Ju, F., Zhao, J.B., et al.: A light cable-driven manipulator developed for aerial robots: structure design and control research. Int. J. Adv. Robot. Syst. **17**(3), 1–14 (2020)
29. Zhang, K., Duan, G.: Output-feedback super-twisting control for line-of-sight angles tracking of non-cooperative target spacecraft. ISA T **94**(1), 17–27 (2019)
30. Munoz, F., Espinoza, E.S., Gonzalez, I., Salazar, S., et al.: Robust trajectory tracking for unmanned aircraft systems using a nonsingular terminal modified super-twisting sliding mode controller. J. Intell. Robot. Syst. **93**(1–2), 55–72 (2019)
31. Zhang, H.Q., Fang, H.R., Zou, Q.: Non-singular terminal sliding mode control for redundantly actuated parallel mechanism. Int. J. Adv. Robot. Syst. **17**(2), 1–13 (2020)
32. Nagamani, G., Karthik, C., Joo, Y.H.: Event-triggered observer-based sliding mode control for t-s fuzzy systems via improved relaxed-based integral inequality. J. Franklin Inst. **357**(14), 9543–9567 (2020)
33. Li, H.Y., Shi, P., Yao, D.Y., Wu, L.G.: Observer-based adaptive sliding mode control for nonlinear markovian jump systems. Automatica **64**, 133–142 (2016)
34. Lu, K., Xia, Y.: Adaptive attitude tracking control for rigid spacecraft with finite-time convergence. Automatica **49**(12), 3591–3599 (2013)
35. Wang, Y.Y., Zhu, K.W., Chen, B., Jin, M.L.: Model-free continuous nonsingular fast terminal sliding mode control for cable-driven manipulators. ISA T **98**(3), 483–495 (2020)
36. Della Santina, C., Bicchi, A., Rus, D.: On an improved state parametrization for soft robots with piecewise constant curvature and its use in model based control. IEEE Robot. Autom. Lett. **5**(2), 1001–1008 (2020)
37. Della Santina, C., Katzschmann, R.K., Bicchi, A., Rus, D.: Model-based dynamic feedback control of a planar soft robot: trajectory tracking and interaction with the environment. Int. J. Robot. Res. **3**(1), 1–24 (2020)
38. Yu, S., Yu, X., Shirinzadeh, B., Man, Z.: Continuous finite-time control for robotic manipulators with terminal sliding mode. Automatica **41**(11), 1957–1964 (2005)
39. Cruz-Zavala, E., Moreno, J.A.: Homogeneous high order sliding mode design: a Lyapunov approach. Automatica **80**(3), 232–238 (2017)
40. Arie, L.: Higher-order sliding modes, differentiation and output-feedback control. Int. J. Control. **76**(9–10), 924–941 (2003)
41. Hendel, R., Khaber, F., Essounbouli, N.: Adaptive high-order sliding mode controller-observer for MIMO uncertain nonlinear systems. Asian J. Control. **00**, 1–21 (2019)
42. An-Min, Z., Kumar, K.D., Zeng-Guang, H., Xi, L.: Finite-time attitude tracking control for spacecraft using terminal sliding mode and chebyshev neural network. IEEE Trans. Syst. Man Cybern. Syst. **41**(4), 950–963 (2011)
43. Liu, J., Sun, M., Chen, Z., Sun, Q.: Super-twisting sliding mode control for aircraft at high angle of attack based on finite-time extended state observer. Nonlinear Dynam. **99**(4), 2785–2799 (2020)
44. Li, B., Qin, K., Xiao, B., Yang, Y.: Finite-time extended state observer based fault tolerant output feedback control for attitude stabilization. ISA T **91**(3), 11–20 (2019)
45. Ullah, I., Pei, H.L.: Fixed time disturbance observer based sliding mode control for a miniature unmanned helicopter hover operations in presence of external disturbances. IEEE Access **8**, 73173–73181 (2020)
46. Wang, H., Shi, L.H., Man, Z.H., Zheng, J.C., et al.: Continuous fast nonsingular terminal sliding mode control of automotive electronic throttle systems using finite-time exact observer. IEEE T Ind. Electron. **65**(9), 7160–7172 (2018)
47. Wang, T., Zhang, Y., Zhu, Y., Zhu, S.: A computationally efficient dynamical model of fluidic soft actuators and its experimental verification. Mechatronics **58**(1), 1–8 (2019)